

Resolving the Structure of Active Sites on Platinum Catalytic Nanoparticles

Lan Yun Chang,^{*,†} Amanda S. Barnard,[‡] Lionel Cervera Gontard,[§] and Rafal E. Dunin-Borkowski[§]

[†]Monash Centre for Electron Microscopy and School of Chemistry, Monash University, Clayton, Victoria, Australia,

[‡]Virtual Nanoscience Laboratory, CSIRO Materials Science and Engineering, Clayton, Victoria, Australia, and [§]Center for Electron Nanoscopy, Technical University of Denmark, DK-2800 Kongens Lyngby, Denmark

ABSTRACT Accurate understanding of the structure of active sites is fundamentally important in predicting catalytic properties of heterogeneous nanocatalysts. We present an accurate determination of both experimental and theoretical atomic structures of surface monatomic steps on industrial platinum nanoparticles. This comparison reveals that the edges of nanoparticles can significantly alter the atomic positions of monatomic steps in their proximity, which can lead to substantial deviations in the catalytic properties compared with the extended surfaces.

KEYWORDS Platinum catalytic nanoparticles, transmission electron microscopy, density functional theory calculations, surface steps

It is now 85 years since Taylor¹ first introduced the concept of “active sites” for heterogeneous catalysis; low-coordinated surface atomic sites that are largely responsible for catalytic reactions. Since then, our understanding of the catalytic properties of extended metal surfaces has been well-established. For example, the atomic structures and roles of defects on extended metal surfaces have been characterized experimentally using techniques such as low energy electron diffraction and scanning tunneling microscopy.^{2–4} From a theoretical perspective, density functional theory has been used to show that the catalytic activity of surface steps is caused by changes in the local electronic structure.^{5,6} While our knowledge of surface defects on extended metal surfaces (model catalysts) has been well established, the actual heterogeneous catalysts that are used in practice are metallic nanoparticles. As the surface-to-bulk ratios of nanoparticles are substantially higher than those of extended surfaces, the electronic structures of their surface defects, and hence their catalytic properties, are expected to be different from their bulk counterparts. However, the characterization of surface defects on nanoparticles is extremely challenging. To date, very little has been deduced about their surface atomic structures. This lack of understanding has been highlighted by a recent theoretical study of the rate of ammonia synthesis when catalyzed by ruthenium nanoparticles.⁷ Moreover as experimental and theoretical studies are rarely conducted in

tandem (on the same type of structure), one must question whether the predictive studies are directly applicable to real catalysts.

Here we present a detailed analysis of the atomic structure of surface defects on Pt nanoparticles using a combination of aberration-corrected transmission electron microscopy (TEM) and density functional theory (DFT). We have used the advanced TEM technique of exit wave restoration to reveal the types of surface defects, including surface steps, on 6 nm carbon-supported Pt nanoparticles. Using this technique, we have measured, for the first time, the quantitative atomic displacements at surface defect sites and performed a detailed comparison with the predictions of ab initio calculations. This comparison has enabled us to gain quantitative insight into the atomic relaxations which take place at the surface defects on nanoparticles, and clearly demonstrates where the two methods correspond and where they do not.

For this type of study, the use of precise techniques (both experimentally and theoretically) is imperative. High-resolution transmission electron microscopy (HRTEM) has the ability to probe the positions of individual atomic sites to the precision of few picometers.^{8–10} In order to directly interpret surface defects, we have utilized the exit wave restoration technique.^{11,12} The advantage of this technique is that, unlike conventional HRTEM imaging, it does not suffer from potentially problematic issues with interpretation. The restored phase of the specimen exit wave function has direct relationship with the projected structure of a thin object. A second advantage of this technique is the enhanced signal-to-noise ratio which allows us to directly image sites that are composed of only a few atoms. We have demonstrated previously that the exit wave restoration technique can be successfully applied to image monatomic steps on the

*To whom correspondence should be addressed. shery.chang@mcm.munash.edu.au.

Received for review: 05/9/2010

Published on Web: 07/28/2010



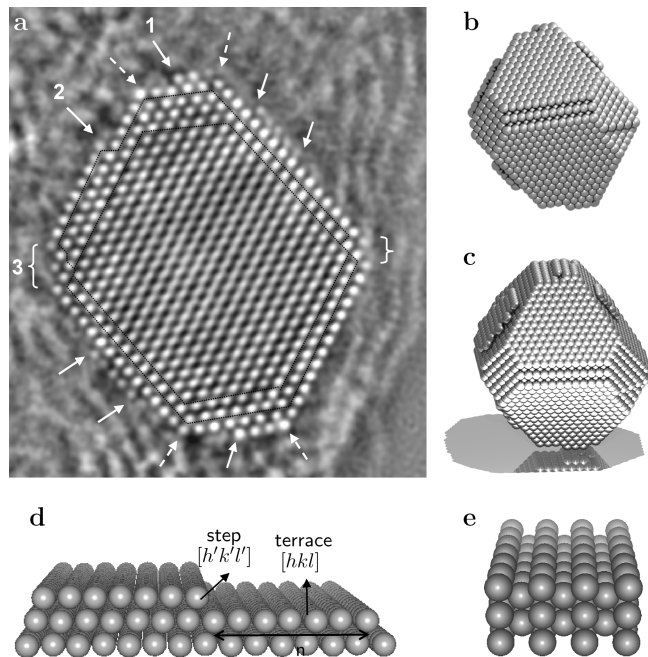


FIGURE 1. Surface defects on a carbon-supported Pt nanoparticle. (a) Experimental phase image of [110]-oriented Pt nanoparticle¹³ exhibiting monatomic surface steps (solid arrows), (111)/(100) edges (dashed arrows), and surface reconstructions on (111)/(111) edges (curly braces). (b) Atomic model of the nanoparticle generated by matching the simulated and the experimental phases. (c) Perspective view of atomic model. (d) Monatomic step notation (S - $n(hkl) \times (h'k'l')$ where (hkl) denotes the terrace plane, $(h'k'l')$ the step plane, and n is the number of atoms on the lower terrace counted from the nanoparticle edge. (e) Model of 1×1 surface reconstruction.

surfaces of industrial Pt nanoparticles¹³ and there have been other reports using this technique to resolve interplanar spacing relaxation on nanoparticles.^{14,15}

The carbon-supported Pt nanoparticles examined in this work were synthesized using the established method described in refs 16 and 17. Figure 1a shows the phase image of a 6 nm Pt nanoparticle, restored from a focal series of 20 high-resolution TEM images (see details in Supporting Information). The phase image shows the Pt nanoparticle in ⟨110⟩ orientation with its surface steps and edges clearly visible. The supporting carbon black is also clearly seen (although the atom positions in the carbon black are less obvious due to the disordered structure).

Several important features regarding the surface steps, edges, and surface reconstructions are noteworthy. First, there are three types of monatomic steps present on the particle, namely, $n(111) \times (100)$, $n(111) \times (111)$, and $n(100) \times (111)$ (following the microfacet notation, $n(hkl) \times (h'k'l')$,¹⁸ illustrated in Figure 1d). The steps on (111) surfaces with (100) and (111) microfacet risers are termed as A- and B-type. Although theoretical calculations of step energies indicate that B-type steps are energetically more stable,^{19,20} our results show that both types are present on the particles. Second, the particle has two types of edges: (111)/(100) edges and (111)/(111) edges. Figure 1a shows that the (111)/(100) edges are sharp, whereas the (111)/(111) edges have

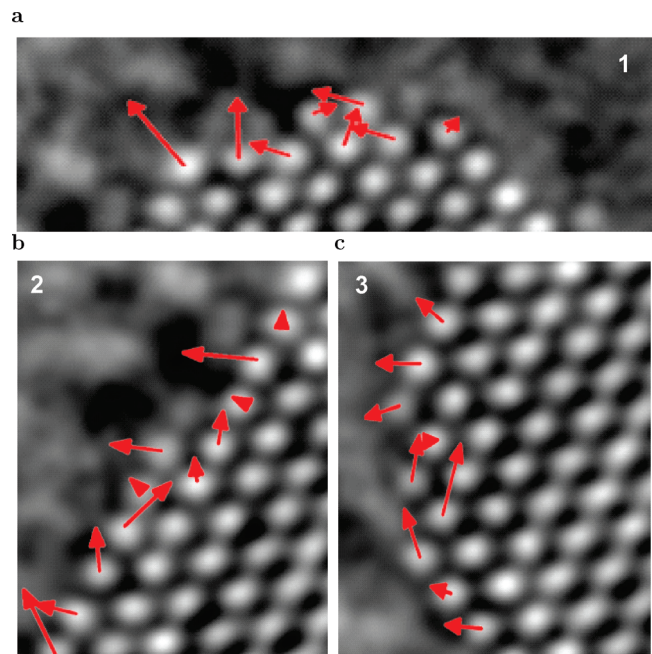


FIGURE 2. Atomic displacements of three representative surface defects on the Pt nanoparticle: (a) monatomic step Pt(S)-2(100) \times (111), marked as region 1 in Figure 1a; (b) monatomic step Pt(S)-5(111) \times (100), marked as region 2; and (c) (110)-(1 \times 1) surface reconstruction, marked as region 3. The red arrows indicate the displacement vectors, which have been magnified 16 times in (a) and (b) and 24 times in (c), for the convenience of visual inspection.

reconstructed into a (110)-(1 \times 1) structure. It should be noted that although a (110)-(1 \times 2) surface reconstruction is the most common structure for extended Pt (110) surfaces,²¹ we have not observed such reconstructions in the nanoparticles examined here.

We now consider in detail the displacements of atoms occurring at the two representative monatomic steps, Pt(S)-2(100) \times (111) and Pt(S)-5(111) \times (100), and the (110)-(1 \times 1) surface reconstruction, marked as regions 1, 2, and 3 in Figure 1a, corresponding to panels a, b, and c of Figure 2, respectively. The atomic displacement vectors were measured with respect to the averaged lattice vectors of the nanoparticle. Several trends in atomic displacements can be drawn from Figure 2. First, the surface atomic sites on (111) and (100) facets generally shift outward with largely varying magnitudes. In particular, the largest atomic displacement is observed on the (111)/(100) edge (the left edge atom in Figure 2a). Second, significant lateral displacements are present at the surfaces of the nanoparticle. The observation of such lateral displacements in the outermost surface layer is in stark contrast to the situation of extended clean Pt surfaces.²

In order to explain the origins of the observed surface atom displacements, we have compared the measured displacements with theoretical calculations of their corresponding, but continuous (edgeless), defects. The calculations were performed from first principles using DFT^{22–26}

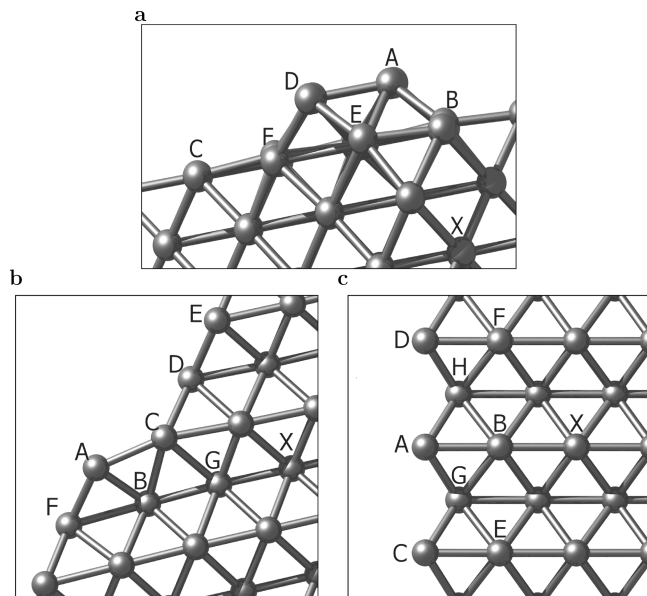


FIGURE 3. Continuous (edgeless) representations of the three surface defects on the Pt nanoparticle calculated using DFT: (a) the monatomic step Pt(S)-2(100) × (111), (b) the monatomic step Pt(S)-5(111) × (100), and (c) the reconstruction (110)-(1 × 1). Each structure has periodicity extending out of the page, and in the in-page directions perpendicular to the free surface.

(details available in the Supporting Information). The results of the DFT calculations are shown in Figure 3, with the slab oriented at the same viewing angle as the facets of the nanoparticle shown in Figure 2.

To facilitate a simple quantitative comparison, Table 1 lists the experimental and theoretical position vectors in terms of their distances and angles with respect to a given reference site. In each case, atoms participating in the defect have been labeled, as shown in Figure 3. In the case of monatomic step Pt(S)-5(111) × (100), there are a number of qualitative similarities between experiment and theory: An extension of the interplanar spacings in the outermost layer is observed; the displacements of the sites in the second atomic layer are negligible (site G). On a quantitative examination, we find very good agreement between experimental and theoretical atomic positions, with the DFT predicting slightly larger outward displacements for the atoms on the outermost (111) surface. In the case of monatomic step Pt(S)-2(100) × (111), the trends between the experimental and theoretical distances are different: DFT predicts shorter distances for all atoms on the (100) surfaces, giving a contraction of the outermost atomic layer (with a significant contraction of the top step atoms (sites A and D)), whereas experimental analysis shows an expansion in the outermost atomic layer. Likewise in the case of the (110)-(1 × 1) surface reconstruction, the DFT predicts shorter atomic distances which amount to slight contraction of the top atoms (sites A, C, and D), whereas experimental analysis shows a slight expansion.

Among the three defects compared above, there is a very good agreement for Pt(S)-5(111) × (100) and less for both

TABLE 1. List of Experimental and Theoretical Distances and Angles of the Position Vectors of the Atomic Sites Labeled as on Figure 3^a

site	experimental value		theoretical value	
	distance	angle	distance	angle
Pt(S)-5(111) × (100)				
A	7.07 ± 0.08	70.1 ± 0.1	7.07	68.9
B	5.36 ± 0.04	56 ± 0.1	5.35	54.9
C	4.44 ± 0.06	79.5 ± 0.1	4.74	81.4
D	4.66 ± 0.06	110.2 ± 0.1	4.85	110.1
E	5.92 ± 0.04	130.6 ± 0.1	5.91	131.8
F	8.03 ± 0.08	55.5 ± 0.1	8.29	54.3
G	2.6 ± 0.06	54.3 ± 0.1	2.69	55.0
Pt(S)-2(100) × (111)				
A	5.75 ± 0.06	103.1 ± 0.1	5.36	103.3
B	3.71 ± 0.06	89.5 ± 0.1	3.62	87.9
C	8.92 ± 0.06	153.8 ± 0.1	8.6	155.8
D	6.74 ± 0.06	124.9 ± 0.1	6.47	126.3
E	4.55 ± 0.04	123.7 ± 0.1	4.64	125.6
F	6.54 ± 0.04	145.7 ± 0.1	6.34	145.2
(110)-(1 × 1)				
A	5.26 ± 0.08	88.8 ± 0.1	5.17	90
B	2.69 ± 0.06	89.4 ± 0.1	2.62	90
C	6.53 ± 0.06	124.5 ± 0.1	6.32	125
D	6.61 ± 0.08	54.3 ± 0.1	6.32	55
E	4.65 ± 0.06	144.2 ± 0.1	4.47	144.1
F	4.63 ± 0.06	34.3 ± 0.1	4.47	35.9
G	4.32 ± 0.06	114.3 ± 0.1	4.41	114.3
H	4.39 ± 0.06	64 ± 0.1	4.41	65.7

^a All distances (in Å) are measured from the reference sites, indicated as “X” on Figure 3. All angles (in degrees) are measured from the axis parallel to the planes of the corresponding surface defect across “X”. The uncertainties in the theoretical distances are consistently ±3 pm, and in the angles ±0.05°, based on a statistical average of like sites following the structural relaxation.

(110)-(1 × 1) reconstruction and Pt(S)-2(100) × (111). Examining the possible discrepancies between the theoretical and experimental atomic models, we find a correlation between the agreement obtained and the proximity of the step to atomic edges. In the case of Pt(S)-5(111) × (100), where good agreement is achieved, the top step atom is five and seven atoms away from the nearest edges. In contrast, the top step atom of Pt(S)-2(100) × (111) is only one and three atoms away from the nearest edges. Similarly, the (110)-(1 × 1) has only two repeating units, with the two top atoms also acting as (111)/(110) edge atoms. Since an edge itself is also a highly strained defect,²⁷ it is not surprising that the presence of edges can have significant influence to the surface steps in the vicinity. The interaction between steps and edges may cause significant electronic structure changes to the surface steps, as demonstrated through the atomic positions of the surface steps in this work, leading to an important consequence in the catalytic property of surface steps on nanoparticles. Since our current understanding of surface steps has been largely based on the experimental and theoretical findings in *continuous* (periodic) systems restricted by the need for translational symmetry, the results of this work highlight the importance of understanding surface defects in *real* (nonperiodic) catalyst materials presented by nanoparticles. Unless edges are included in elec-

tronic structure simulations (as well as surface steps) the predictions of catalytic activity arising from some expertly conducted DFT studies may still be misleading, especially when one introduces surface adsorption of atomic or molecular species from a surrounding gaseous or liquid environment. These considerations will form a path of future research.

Acknowledgment. L.Y.C., L.C.G., and R.D.B. gratefully acknowledge Professor Angus Kirkland and Dr. Crispin Hetherington for the use of the aberration-corrected JEOL 2200FS at Oxford University, U.K. Dr. Dogan Ozkaya, Johnson-Matthey Research Centre, U.K., is also acknowledged for supplying carbon supported Pt nanoparticles. A.S.B. gratefully acknowledges support from the ARC (DP0986752), L'Oréal Australia, and computational resources from the National Computing Infrastructure (NCI) national facility (under MAS Grant p00). Fruitful discussions with Dr. Christian Dwyer are gratefully acknowledged.

Supporting Information Available. Detailed description of the experimental imaging conditions, exit wave restoration, atomic position and atomic displacement measurements, and the DFT calculations. This material is available free of charge via the Internet at <http://pubs.acs.org>.

REFERENCES AND NOTES

- (1) Taylor, H. S. *Proc. R. Soc. London, Ser. A* **1925**, *108*, 105.
- (2) Blakely, J. M.; Eizenberg, M. Morphology and composition of crystal surface. In *Chemical physics of solid surfaces and heterogeneous catalysis*; King, D. A., Woodruff, D. P., Eds.; Elsevier: Amsterdam, 1982; Vol. 1.
- (3) Thomas, J. M. *Principles and practice of heterogeneous catalysis*; VCH: Cambridge, 1997.
- (4) Zambelli, T.; Wintterlin, J.; Trost, J.; Ertl, G. *Science* **1996**, *273*, 1688–1690.
- (5) Greeley, J.; Nørskov, J. K.; Mavrikakis, M. *Annu. Rev. Phys. Chem.* **2002**, *53*, 319–348.
- (6) Nørskov, J. K.; Scheffer, M.; Toulhoat, H. *MRS Bull.* **2006**, *31*, 669–674.
- (7) Honkala, K.; Hellman, A.; Remediakis, I. N.; Logadottir, A.; Caelsson, A.; Dahl, S.; Christensen, C. H.; Nørskov, J. K. *Science* **2005**, *307*, 555–558.
- (8) van Aert, S.; Chang, L. Y.; Bals, S.; Kirkland, A. I.; van Tendeloo, G. *Ultramicroscopy* **2009**, *109*, 237–246.
- (9) Bals, S.; van Aert, S.; van Tendeloo, G.; Ávila-Brande, D. *Phys. Rev. Lett.* **2006**, *96*, No. 096106–096110.
- (10) Meyer, R. R.; Sloan, J.; Dunin-Borkowski, R. E.; Kirkland, A. I.; Novotny, M. C.; Bailey, S. R.; Hutchison, J. L.; Green, M. L. H. *Science* **2000**, *289*, 1324–1326.
- (11) Meyer, R. R.; Kirkland, A. I.; Saxton, W. O. *Ultramicroscopy* **2004**, *99*, 115–123.
- (12) Chang, L. Y.; Kirkland, A. I. *Microsc. Microanal.* **2006**, *12*, 469–475.
- (13) Gontard, L. C.; Chang, L. Y.; Hetherington, C. D.; Kirkland, A. I.; Ozkaya, D.; Dunin-Borkowski, E. R. *Angew. Chem., Int. Ed.* **2007**, *46*, 3683–3685. Copyright Wiley-VCH Verlag GmbH & Co. KGaA. Reproduced with permission.
- (14) Wang, R. M.; Dmitrieva, O.; Farle, M.; Dumpich, G.; Ye, H. Q.; Poppa, H.; Kilaas, R.; Kisielowski, C. *Phys. Rev. Lett.* **2008**, *100*, No. 017205.
- (15) Kawasaki, T.; Takai, Y.; Shimizu, R. *Appl. Phys. Lett.* **2001**, *79*, 3509–3511.
- (16) Ralph, B. T. R.; Hogarth, M. P. *Platinum Metal Rev.* **2002**, *46*, 3.
- (17) Ozkaya, D.; Thompsett, D.; Goodlet, G.; Spratt, S.; Ash, P.; Boyd, D. *Inst. Phys. Conf. Ser.* **2003**, *179*, 2.
- (18) Lang, B.; Joyner, R. W.; Somorjai, G. A. *Surf. Sci.* **1972**, *30*, 440–453.
- (19) Vitos, L.; Ruban, A. V.; Skriver, H. L.; Kollár, J. *Surf. Sci.* **1998**, *411*, 186–202.
- (20) Vitos, L.; Skriver, H. L.; Kollár, J. *Surf. Sci.* **1999**, *425*, 212–223.
- (21) Sowa, E. C.; Van Hove, M. A.; Adams, D. L. *Surf. Sci.* **1988**, *199*, 174.
- (22) Perdew, J. P.; Burke, K.; Ernzerhof, M. *Phys. Rev. Lett.* **1996**, *77*, 3865–3868.
- (23) Kresse, G.; Hafner, J. *Phys. Rev. B* **1993**, *47*, 558–561.
- (24) Kresse, G.; Furthmüller, J. *Phys. Rev. B* **1996**, *54*, 11169–11186.
- (25) Blöchl, P. E. *Phys. Rev. B* **1994**, *50*, 17953–17979.
- (26) Kresse, G.; Joubert, D. *Phys. Rev. B* **1999**, *59*, 1758–1775.
- (27) Johnson, C. L.; Snoeck, E.; Ezcurdia, M.; Rodriguez-González, B.; Pastoriza-Santos, I.; Liz-Marzán, L. M.; Hjøtch, M. J. *Nat. Mater.* **2007**, *7*, 120–124.